

Manifold Regularized Tucker Decomposition Approach for Spatiotemporal Traffic Data Imputation

Wenwu Gong, Zhejun Huang, and Lili Yang

Abstract—Spatiotemporal traffic data imputation (STDI), estimating the missing value from partially observed traffic data, is an inevitable and challenging task in data-driven intelligent transportation systems (ITS). Due to the traffic data's multidimensionality, we transform the traffic matrix into the 3rd-order tensor and propose an innovative manifold regularized Tucker decomposition (ManiRTD) model for STDI. ManiRTD considers the sparsity of the Tucker core tensor to constrain the low rankness and employs manifold regularization and the Toeplitz matrix to enhance the model performance. We address the ManiRTD model through a block coordinate descent framework under alternating proximal gradient updating rules with convergence-guaranteed. Numerical experiments on real-world spatiotemporal traffic datasets (STDs) demonstrate that our proposed model is superior to the other baselines under various missing scenarios.

Index Terms—Spatiotemporal traffic data imputation, regularized Tucker decomposition, spatial similarity, temporal variation, alternating proximal gradient.

I. INTRODUCTION

SPATIOTEMPORAL traffic data analysis is vital for road traffic control with the development and application of intelligent transportation systems (ITS). For example, the road loop sensors record traffic state, including traffic speed, traffic flow, and occupancy rate; the cars equipped with GPS (internet traffic data) record subjects' movement from an origin to a destination, involving pair, time, and day modes. Both of them contain helpful information for traffic networks and route planning. Unfortunately, the missing data problem is inevitable due to communication malfunctions, transmission distortions, or adverse weather conditions [1]. Consequently, the spatiotemporal traffic data imputation (STDI) is unavoidable and urgently required in ITS.

Plenty of imputation methods have been proposed to deal with the missing data problem, such as statistical-based methods [2] and deep learning-based [3] methods. However, these methods either have low accuracy or lack interpretability. Due to spatiotemporal traffic data's multidimensional structure and large-scale nature [4], the low-rank tensor completion methods have been well developed. On the one hand, the low-rank tensor approximation (LRTA) model has proven highly effective in STDI from a theoretical and application-specific perspective [5], [6]. On the other hand, characterizing spatiotemporal correlations is the basic modeling idea of STDI [7], [8]. Hence, combining low rankness (long-term trends) and spatiotemporal correlations (short-term patterns) in traffic data is still challenging to improve imputation performance.

A. Motivations

This paper aims to capture spatiotemporal patterns from partially observed STDs via a factorization model and then use them to estimate the missing value accurately. Because low rankness provides long-term trends for the traffic data, the LRTA-based optimization model (referred to as the Tucker decomposition model in this paper) with spatiotemporal regularization is used for the STDI problem. The motivations of our proposed model are three folds:

Firstly, the multidimensional array of STDs contains rich information. For example, traffic speed data in adjacent sensors show similar patterns and present temporal correlation properties [9]. The 2-dimensional traffic matrix imputation ignores the multidimensional nature and cannot deal with high missing rate scenarios [10], especially for the structure missing scenario. Reshaping the original traffic data into a high-order tensor and capturing the underlying multidimensionality in the low-rank subspace to capture the spatiotemporal characteristic is essential.

Minimizing the tensor rank is generally challenging since it is a nonconvex function. Matrix nuclear-norm minimization and tensor rank minimization suffers from computation burden [4]. Instead of flattening tensors into matrices and then using the matrix rank techniques, the Tucker decomposition model preserves the multidimensional nature of the STD and extracts the hidden patterns [11]. Thus, the low-rank Tucker decomposition is a suitable model for STDI.

Thirdly, when the missing ratio is high, the imputation accuracy of low-rank models severely degrade [12]. Thus, we should consider spatiotemporal constraints in the LRTA framework for STDI. Such as, regularization-based methods are used to reflect the spatial and temporal correlations [9], [13].

B. Challenges and Contributions

Though low-rank tensor completion is a hot topic for STDI, the problem is still open and needs better addressed, especially considering the following challenges.

The first challenge is how to leverage the low-rank structure of the STD (i.e., long-term trends). It remains to propose a data-driven Tucker model to determine the traffic data structures. In addition, the decomposition model requires a predefined rank as a hyperparameter. Still, finding the optimal rank for Tucker decomposition in advance is difficult. Considering the spatiotemporal correlations (i.e., short-term patterns)

of the STD, the third challenge is how to encode the “local” consistency to low-rank approximation models and enhance the imputation performance.

This paper proposes an innovative tensor decomposition model called ManiRTD for STDI to answer the above limitations. We summarize the main contributions as follows:

- 1) To capture the traffic data structure, we reshape the matrix-based data in a 3rd/4th tensor form and show the 3rd-order tensor structure covers richer spatial and temporal information;
- 2) We propose ManiRTD to characterize long-term trends and short-term patterns in STDs. More specifically, the proposed model promotes low rankness by contrasting the sparsity of the Tucker core tensor. Additionally, ManiRTD employs manifold regularization and Toeplitz matrix terms to factor matrices of the Tucker decomposition to characterize the spatiotemporal correlations and enhance the model performance;
- 3) The proposed model is a highly nonconvex optimization problem with coupled variables. We address the ManiRTD through Block Coordinate Decent (BCD) framework to decouple the objective function. More specifically, we apply an alternating proximal gradient (APG) method to find the optimal solutions, where the algorithm updates the Tucker decomposition with closed-form solutions;
- 4) We verify the importance of spatiotemporal constraints in ManiRTD on two real-world STDs. A comprehensive comparative study with baselines is also conducted to demonstrate the effectiveness of ManiRTD. With the free-hyperparameters tuning, we demonstrate that ManiRTD performs better in real-world traffic imputation problems under different types of missing scenarios.

We organize the rest of the paper as follows. Section II discusses the related work on STDI. Section III introduces the notations and preliminaries in this paper. Section IV proposes the model framework, and Section V designs the algorithm of ManiRTD. In Section VI, we evaluate the performance of our methods on extensive experiments and compare them with some baseline approaches. The last section concludes this paper and presents future work.

II. RELATED WORK

Numerous time series imputation methods have been developed in the last two decades, especially for STDI [14]. From the model-building perspective, these methods can be divided into machine- and low-rank learning-based. Because STD has spatial similarity and temporal variation characteristics, many studies have proven that the low-rankness assumption combined with the spatiotemporal information method performs better than other existing methods for STDI [4], [9]. So, the low-rank tensor learning methods for STDI are discussed in detail in the following section.

A. Low-rankness

Low-rank property, which depicts the inherent correlations in real-world datasets, is an essential and significant assumption

in the completion problem. There are two categories of low-rank models to estimate the missing data problems: norm minimization and low-rank approximation. Regarding norm minimization, Candes et al. [15] proposed the trace norm approximation to precisely estimate the missing matrix data. Liu et al. [16] extended the matrix case to the tensor by proposing the nuclear norm for the image inpainting problem. Tan et al. [17] applied the low-rank tensor nuclear norm minimization method to impute the spatiotemporal traffic flow.

To avoid using the computationally expensive singular value decomposition (SVD) in unfolding matrix norm minimization, Chen et al. [1] proposed a Tucker decomposition model based on the truncated singular values of each factor matrix to exploit the low rankness in STD. Furthermore, Yokota et al. [18] showed that the rank increment strategy is sufficient when a lower m-rank approximation initializes the tensor than its target m-rank in Tucker-based completion applications.

It can be seen that a significant difference between these two approximation methods is the way that they make decisions about low rankness. Compared with nuclear norm minimization with rank estimation, on the one hand, the low-rank approximation model can avoid the high-cost unfolding matrix SVD under a given m-rank or small-size factor matrices. On the other hand, the nuclear norm minimization cannot impose spatiotemporal constraints directly on factor matrices [13]. So, it is reasonable to believe that the low-rank approximation model is more appropriate for the STDI task.

B. Decomposition Model

Low-rank Tucker and CANDECOMP/PARAFAC (CP) decomposition, a high-order matrix factorization extension, has received increasing attention in spatiotemporal traffic data analysis. On the one hand, considering the sensory traffic matrix data, many papers applied the spatiotemporal Hankel operator to capture the low-rank structure by transforming the original incomplete matrix to a 4th-order tensor [10], [19]. This transformer captures the spatiotemporal information in a purely data-driven manner but is time-consuming. On the other hand, many papers used Tucker and CP decomposition models for STDI. For example, Tan et al. [20], [21] proposed a Tucker decomposition-based model to estimate the missing traffic speed, guaranteeing accurate performance. Wang et al. [22] proposed a context-aware Tucker decomposition approach to predict the drivers’ travel time on the main city roads. Chen et al. [23] proposed a Bayesian augmented CP decomposition model for traffic data analysis, combining domain knowledge to enhance the imputation performance. However, estimating the minimum rank of CP decomposition in practice takes much work. Moreover, the Tucker decomposition model can discover spatiotemporal patterns by interpreting the factor matrices [1]. So, this paper focuses on the Tucker decomposition model for spatiotemporal traffic data imputation.

C. Regularized Tucker Decomposition

Tucker decomposition models can be used to preserve high-order tensor data global information. Still, they may interpret local similarity (such as spatiotemporal information in traffic

data) inadequately and obtain low performance for STDI. Many studies have reported that using a low-rank Tucker decomposition model is insufficient for the case where the high-order tensors do not have an explicit low-rank structure [24], [25]. To circumvent this problem, one of the most popular methods is to add an l_2 norm regularizer on the factor matrices of the Tucker decomposition. Furthermore, Rose et al. [7] proposed a unified low-rank tensor learning framework considering spatial similarity by constructing a Laplacian regularizer for spatiotemporal data analysis.

Considering the spatiotemporal correlations in traffic data, many papers studied the local similarity by leveraging some regularization techniques, such as l_2 smoothness [1], manifold regularization [8], temporal regularization [26], and sparsity [27]. For example, Zhang et al. [28] combined Tucker decomposition with the l_2 norm regularization of the factor matrix to detect and estimate traffic flows in the Automatic Number Plate Recognition system. Wang et al. [29] proposed a graph-regularized non-negative Tucker decomposition model to discover the interpretable traffic pattern from urban traffic flows. Besides, Chen et al. [4] introduced the temporal regularization term into the low-rank tensor completion framework to accomplish the traffic speed imputation. Goulart et al. [30] applied the orthogonal Tucker model with tensor core thresholding to adjust the core tensor size and introduced a feedback mechanism to enhance the traffic flow imputation performance. Most of these approaches are designed based purely on spatial or temporal correlation and have a low data imputation performance. Wu et al. [24] proposed a modified CP decomposition framework that fuses the l_2 norm constraint, sparseness, and total variation to capture more spatiotemporal features in the STDI problem. Also, Pan et al. [25] proposed a sparse enhanced Tucker decomposition model in tensor completion task, where the low-rank regularization terms of factor matrices combined with sparse core tensor exploit inherent global information and a general Toeplitz matrix is used to characterize the periodicity in STD.

However, to our knowledge, most papers still need to fully consider the global and local patterns simultaneously, i.e., low-rankness, and the hidden similarity structure of factor matrices in the Tucker model. The proposed ManiRTD addresses these properties in a tensor object by reshaping the traffic matrix data in a high-order spatiotemporal tensor form. Then, ManiRTD exploits the long-term traffic trends using a low-rank sparse Tucker model and captures the short-term patterns with given spatiotemporal priors, including manifold and Toeplitz regularizations. Our experiment results demonstrate that ManiRTD performs better in spatiotemporal traffic data imputation.

III. PRELIMINARIES

We review some related concepts of Tucker decomposition as follows and present all notations used in this paper in Tab. I. We refer [6] for more details of preliminaries.

A. Notations

A tensor is a multidimensional array where the order of the tensor is the number of dimensions, also called the mode.

TABLE I
NOTATIONS

$\mathcal{X}, \mathbf{U}, \alpha$	A tensor, matrix and real value, respectively.
$\mathbb{R}_{+}^{I_1 \times I_2 \times \dots \times I_N}$	Set of N-th order nonnegative array.
$\mathbf{U} \geq 0$	Nonnegative matrix \mathbf{U} , i.e., $u_{ij} \geq 0, \forall i, j$.
$\mathcal{P}_{+}(\mathbf{U})$	Operator yielding a nonnegative matrix of $u_{ij} = \max(u_{ij}, 0), \forall i, j$.
$\mathcal{S}_{\mu}(x)$	Shrinkage operator with μ in component-wise
$\Omega, \bar{\Omega}$	Observed index set and its complement.
\mathcal{X}_{Ω}	Observed entries supported on the observed index
\mathcal{H}	MDT operator.
\times_n	Mode-n product.
\otimes, \odot	Kronecker product and Hadamard product.
$\ \cdot\ _F$	Frobenius norm.
$\mathbf{X}_{(n)}$	Mode-n unfolding of tensor \mathcal{X} .
tr	Matrix trace operator.

Throughout this paper, we use calligraphy font for tensors, such as $\mathcal{X} \in \mathbb{R}^{I_1 \times I_2 \times \dots \times I_N}$, whose element is denoted as x_{i_1, i_2, \dots, i_n} . The bold uppercase letters for matrices, such as $\mathbf{U} \in \mathbb{R}^{I_1 \times I_2}$, bold lowercase letters for vectors, such as $\mathbf{a} \in \mathbb{R}^{I_1}$, and lower case for scalars, such as α, β .

The Frobenius norm of a tensor is defined as

$$\|\mathcal{X}\|_F = \sqrt{\sum_{i_1=1}^{I_1} \dots \sum_{i_n=1}^{I_n} x_{i_1 \dots i_n}^2}.$$

We denote the mode- n unfolding (i.e., matricization) of an N -order tensor \mathcal{X} by $\mathbf{X}_{(n)} \in \mathbb{R}^{I_n \times \prod_{j \neq n} I_j}$.

The Tucker decomposition can be viewed as a higher-order principal component operator that minimizes the error in learning the projection on the subspace. Given a tensor $\mathcal{X} \in \mathbb{R}^{I_1 \times I_2 \times \dots \times I_N}$, it can be decomposed into a core tensor $\mathcal{G} \in \mathbb{R}^{r_1 \times r_2 \times \dots \times r_N}$ multiplying a matrix $\mathbf{U}_n \in \mathbb{R}^{I_n \times r_n}$ along each mode, i.e., $\mathcal{X} = \mathcal{G} \times_1 \mathbf{U}_1 \dots \times_N \mathbf{U}_N = \mathcal{G} \times_{n=1}^N \mathbf{U}_n$. The core tensor \mathcal{G} can be regarded as a compressed version of \mathcal{X} if r_1, r_2, \dots, r_N are significantly smaller than I_1, I_2, \dots, I_N .

Based on the matrix Kronecker product \otimes , we can represent the Tucker decomposition by

$$\mathbf{X}_{(n)} = \mathbf{U}_n \mathbf{G}_{(n)} \mathbf{V}_n^T$$

where $\mathbf{V}_n = (\mathbf{U}_N \otimes \dots \otimes \mathbf{U}_{n+1} \otimes \mathbf{U}_{n-1} \otimes \dots \otimes \mathbf{U}_1)$. Furthermore, it is not difficult to verify that $\text{vec}(\mathcal{X}) = (\mathbf{U}_N \otimes \dots \otimes \mathbf{U}_n \otimes \dots \otimes \mathbf{U}_1) \text{vec}(\mathcal{G}) = \otimes_{n=1}^N \mathbf{U}_n \text{vec}(\mathcal{G})$.

Finally, for a given tensor $\mathcal{X} \in \mathbb{R}^{I_1 \times I_2 \times \dots \times I_N}$ and observed index set Ω , we define \mathcal{X}_{Ω} as a projector that keeps the nonzero terms and leaves the other values as zero values, i.e.,

$$\mathcal{X}_{\Omega} := \begin{cases} x_{i_1 i_2 \dots i_n}, & \text{if } (i_1, i_2, \dots, i_n) \in \Omega \\ 0, & \text{otherwise.} \end{cases}$$

B. Problem Definition

The spatiotemporal traffic data (STD), collected from M sensors over J days with I time points, is presented as a multivariate time series matrix $\mathbf{Y} \in \mathbb{R}^{M \times I \times J}$ in Fig. 1 (a). Here, we denote the partially observed matrix as \mathbf{Y}_{Ω} with the observed index set Ω . Guided by Chen et. al. [4] and Wang et. al. [10], the STDI can be approximated by a low-rank tensor completion, where the tensorization operator transforms the matrix data into a higher-order tensor structure. In this paper,

we introduce the MDT operator [18] \mathcal{H} to reshape the traffic matrix into 3rd/4th-order tensors and formulate a Low-rank Tucker approximation problem, shown in Fig. 1 (b). The low-rank Tucker decomposition model captures the global long-term trends and applies manifold and Toeplitz regularizations to model the short-term patterns to enhance the imputation performance. Conversely, the inverse operator $\hat{\mathbf{Y}} = \mathcal{H}^{-1}(\hat{\mathcal{X}})$ converts the reconstructed tensor into the original traffic matrix and then estimates the missing values.

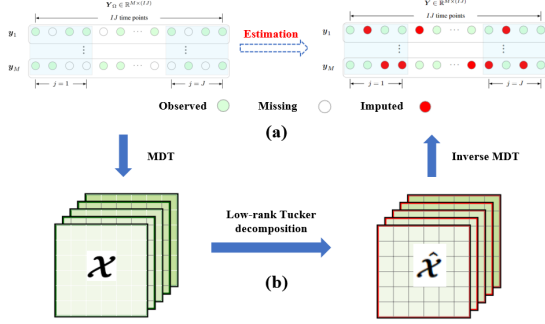


Fig. 1. Spatiotemporal traffic data collected from ITS. (a) Matrix representation. (b) Low-rank Tucker approximation based on the high-order tensor.

Mathematically, we illustrate our proposal by minimizing the following objective function:

$$\begin{aligned} \underset{\mathcal{G}; \{\mathbf{U}_n\}; \mathcal{X}}{\text{minimize}} \quad & \frac{1}{2} \|\mathcal{X} - \mathcal{G} \times_{n=1}^N \mathbf{U}_n\|_F^2 + \mu(\{\mathbf{U}_n\}) + \beta \|\mathcal{G}\|_1 \\ \text{s.t.} \quad & \mathcal{X}_\Omega = \mathcal{H}(\mathbf{Y}_\Omega) \end{aligned} \quad (1)$$

where $\mu(\cdot)$ is the user-defined spatiotemporal constraint, and β is a tradeoff parameter to compromise the role of the core tensor. Under different missing scenarios, we update \mathcal{X} by the rule

$$\hat{\mathcal{X}} = \mathcal{X}_\Omega + \{\hat{\mathcal{G}} \times_1 \hat{\mathbf{U}}_1 \cdots \times_N \hat{\mathbf{U}}_N\}_{\bar{\Omega}}, \quad (2)$$

and impute the spatiotemporal traffic matrix by $\hat{\mathbf{Y}} = \mathcal{H}^{-1}(\hat{\mathcal{X}})$.

IV. PROPOSED MODEL

This section details the formulation of STDI using the ManiRTD, which consists of the sparsity of the Tucker core tensor, temporal variations, and spatial similarity of the Hankel tensor.

A. Spatiotemporal Constraints

Tucker decomposition with a sparse core tensor captures the long-term trends for the traffic tensor object. However, the characteristics of STD, such as the spatial mode similarity in the different road links (road network topology) and the temporal mode varied from time to time (time series correlation), cannot be fully exploited.

Noted in Wang et. al. [13], traffic data collected by nearby sensors tend to have similar characteristics, which reflects spatial similarity. In addition, traffic data is often non-stationary in the time dimension, and the non-missing traffic data values have a continuous trend and show a temporal variation [31]. Nonetheless, most imputation methods consider time-varying without considering the spatial similarity in the STDI. Guided

by Chen et. al. [1], we consider the factor matrices regularization for exploiting spatiotemporal correlations in STDI. In this paper, we address the spatiotemporal property relying on the manifold regularization and Toeplitz constraint matrix, which leads to better performance for the STDI problem.

1) *Manifold regularization*: it is to deal with non-linear data dimension reduction, which assures that if two data objects are geometrically close under the manifold, they should also be close to each other after dimensionality reduction [11]. Given the similarity matrix $\mathbf{W} \in \mathbb{R}^{N \times N}$ for data $\mathbf{X} \in \mathbb{R}^{I \times N}$, where $0 \leq w_{ij} \leq 1$, $i, j = 1, \dots, N$, we can use (3), the manifold regularization term, to capture an optimal low-dimensional representation \mathbf{U} for given data \mathbf{X} .

$$\sum_{i=1}^N \sum_{j=1}^N w_{ij} \|\mathbf{u}_i - \mathbf{u}_j\|_2^2 = \text{tr}(\mathbf{U}^T \mathbf{L} \mathbf{U}), \quad \mathbf{L} = \mathbf{D} - \mathbf{W} \quad (3)$$

where \mathbf{u}_i is the column vector of \mathbf{U}^T and $\mathbf{D} \in \mathbb{R}^{N \times N}$ is a diagonal matrix with diagonal elements $d_{ii} = \sum_{j=1}^N w_{ij}$, $i = 1, \dots, N$. Note that \mathbf{L} is a Laplacian matrix designed by similarity matrix \mathbf{W} , which enforces the smoothness of the low-dimensional feature \mathbf{U} [12].

Since the high-dimensional spatiotemporal traffic data usually reside in low-dimensional submanifolds, manifold regularization can be used to learn the spatial similarity and avoid model overfitting. More specifically, the proposal ManiRTD uses the k-nearest neighbors algorithm (KNN) to select p nearest neighbors for each unfolding image tensor and then construct the similarity matrix \mathbf{W} to represent the neighbor connections.

The most important parts of manifold regularization are two folds: the Laplacian matrix construction and similarity matrix calculation. In this paper, we apply different strategies to do that [32]. On the one hand, we suppose that the intrinsic manifold is located in the convex envelope of the previously given manifold Laplacian matrices $\{\mathbf{L}_1, \dots, \mathbf{L}_K\}$, such that, the ensemble graph Laplacians is denoted as a linear combination of K candidate Laplacians:

$$\mathbf{L} = \sum_{k=1}^K \tau_k \mathbf{L}_k, \quad \text{s.t.} \quad \sum_{k=1}^K \tau_k = 1, \tau_k \geq 0, \quad (4)$$

where τ_k is the combined weight of k -th graph Laplacian and the constraint $\tau_k \geq 0$ is used to avoid negative contribution. On the other hand, we use kernel weighting to define the similarity matrix. For each data point x_i belongs to unfolding matrix \mathbf{X} , if nodes i and j are connected, the kernel weight is defined as (5)

$$w_{ij} = e^{-(\|x_i - x_j\|^2)/\sigma^2}, \quad (5)$$

where σ^2 denotes the divergence, and we set $\sigma^2 = 1$ in our experiments.

2) *Toeplitz regularization*: it is to capture the continuity change characteristics in the time dimensional. Considering the non-stationary in the temporal dimension, the original traffic data is often correlated at adjacent time points. Consequently, we use the first-order Toeplitz constraint matrix

\mathbf{T} = Toeplitz(0, 1, -1), i.e., $\|\mathbf{T}\mathbf{U}\|_F^2$ to characterize the time continuity of traffic data in this paper.

$$\mathbf{T} = \begin{pmatrix} 1 & -1 & \cdots & 0 & 0 & 0 \\ 0 & 1 & \cdots & 0 & 0 & 0 \\ 0 & 0 & \cdots & -1 & 0 & 0 \\ \vdots & \vdots & \ddots & \vdots & \vdots & \vdots \\ 0 & 0 & \cdots & 0 & 1 & -1 \\ 0 & 0 & \cdots & 0 & 0 & 1 \end{pmatrix}. \quad (6)$$

B. Manifold Regularized Tucker Decomposition Model

Let $\mathcal{X}^0 \in \mathbb{R}^{I_1 \times I_2 \times \cdots \times I_N}$ be the spatiotemporal traffic tensor under the missing scenario, and Ω is the set of indexes corresponding to the observations. Based on the model (1) and the aforementioned spatiotemporal constraints, we consider the following optimization problem

$$\begin{aligned} & \underset{\mathcal{G}; \{\mathbf{U}_n\}; \mathcal{X}}{\text{minimize}} \quad \mathbb{F}(\mathcal{G}, \{\mathbf{U}_n\}, \mathcal{X}) \\ & \triangleq \left\{ \frac{1}{2} \|\mathcal{X} - \mathcal{G} \times_{n=1}^N \mathbf{U}_n\|_F^2 + \beta \|\mathcal{G}\|_1 \right. \\ & \quad \left. + \frac{\alpha}{2} \left(\sum_{n=1}^j \text{tr}(\mathbf{U}_n^T \mathbf{L}_n \mathbf{U}_n) + \sum_{n=j+1}^N \|\mathbf{T}\mathbf{U}_n\|_F^2 \right) \right\} \\ & \text{s.t. } \mathbf{U}_n \in \mathbb{R}_+^{I_n \times I_n}, n = 1, \dots, N \text{ and } \mathcal{X}_\Omega = \mathcal{X}_\Omega^0, \end{aligned} \quad (7)$$

where α, β are positive penalty parameters, \mathbf{L}_n captures the spatial similarity, and \mathbf{T} encodes the temporal variation. Note that the non-negativity constraints on the factor matrix ensure explaining traffic patterns more intuitively [33]. We name the model in (7) as the Manifold Regularization Tucker Decomposition (ManiRTD) method, which exploits the spatiotemporal correlations and low rankness of sensory traffic matrix data simultaneously.

V. SOLVING MANIRTD MODEL

To solve the complicated optimization problems (7), we adapt the BCD framework, that is, only updating $\{\mathbf{U}_n\}$ or \mathcal{G} while remaining the others fixed until convergence. Hence, the problem of the ManiRTD is divided into $N + 1$ subproblems and can be solved by the APG updating rule. Furthermore, we present the convergence and computational results for our proposed ManiRTD model.

A. Optimization for the ManiRTD Model

The ManiRTD can be treated as the regularized block multi-convex optimization problem [34] (see Appendix A), where the prox-linear operator can be used to solve that. The details are shown in Appendix A.

Firstly, we unfold (7) in mode- n for given tensor \mathcal{X} , then the latent factor matrices multi-convex optimization subproblems are given as the following three types.

- Basic nonnegative matrix factorization.

$$\underset{\mathbf{U}_n \geq 0}{\text{minimize}} \quad \ell(\mathbf{U}_n) = \frac{1}{2} \|\mathbf{X}_{(n)} - \mathbf{U}_n \mathbf{G}_{(n)} \mathbf{V}_n^T\|_F^2 \quad (8)$$

where $\mathbf{V}_n = \otimes_{p=N, p \neq n}^1 \mathbf{U}_p$.

- Manifold regularization on factor matrix.

$$\underset{\mathbf{U}_n \geq 0}{\text{minimize}} \quad \ell(\mathbf{U}_n) = \frac{1}{2} \|\mathbf{X}_{(n)} - \mathbf{U}_n \mathbf{G}_{(n)} \mathbf{V}_n^T\|_F^2 + \frac{\alpha}{2} \text{tr}(\mathbf{U}_n^T \mathbf{L}_n \mathbf{U}_n) \quad (9)$$

where $\mathbf{L}_n = \mathbf{D}_n - \mathbf{W}_n$ represents the Laplacian matrix.

- Temporal regularization on factor matrix.

$$\underset{\mathbf{U}_n \geq 0}{\text{minimize}} \quad \ell(\mathbf{U}_n) = \frac{1}{2} \|\mathbf{X}_{(n)} - \mathbf{U}_n \mathbf{G}_{(n)} \mathbf{V}_n^T\|_F^2 + \frac{\alpha}{2} \|\mathbf{T}\mathbf{U}_n\|_F^2 \quad (10)$$

where \mathbf{T} is a self-defined temporal constraint matrix.

Proposition 1: The objective function of subproblems (8) - (10) are differentiable and convex. Furthermore, the gradients $\nabla_{\mathbf{U}_n} \ell(\mathbf{U}_n)$ are both Lipschitz continuous with the Lipschitz constant

$$L_{\mathbf{U}_n} = \begin{cases} \left\| \mathbf{G}_{(n)} \mathbf{V}_n^T \mathbf{V}_n \mathbf{G}_{(n)}^T \right\|_2 + \alpha \|\mathbf{L}\|_2, & \text{Manifold} \\ \left\| \mathbf{G}_{(n)} \mathbf{V}_n^T \mathbf{V}_n \mathbf{G}_{(n)}^T \right\|_2 + \alpha \|\mathbf{T}^T \mathbf{T}\|_2, & \text{Temporal} \\ \left\| \mathbf{G}_{(n)} \mathbf{V}_n^T \mathbf{V}_n \mathbf{G}_{(n)}^T \right\|_2, & \text{otherwise} \end{cases}$$

Based on *Proposition 1*, we use a prox-linear updating scheme, i.e., (11), to obtain the stationary point of the projection matrices (shown in (15)). Appendix A contains the induction of updating rules and detailed proof of *Proposition 1*.

$$\begin{aligned} \hat{\mathbf{U}}_n = \underset{\mathbf{U}_n \geq 0}{\text{argmin}} \quad & \Psi(\mathbf{U}_n, \tilde{\mathbf{U}}_n) = \left\langle \nabla_{\mathbf{U}_n} \ell(\tilde{\mathbf{U}}_n), \mathbf{U}_n - \tilde{\mathbf{U}}_n \right\rangle \\ & + \frac{L_{\mathbf{U}_n}}{2} \|\mathbf{U}_n - \tilde{\mathbf{U}}_n\|_F^2, \end{aligned} \quad (11)$$

where $\tilde{\mathbf{U}}_n$ denotes the extrapolated point.

Secondly, we update the subproblem \mathcal{G} using the vectorization optimization problem (12)

$$\begin{aligned} & \underset{\mathcal{G}}{\text{minimize}} \quad \frac{1}{2} \|\text{vec}(\mathcal{X}) - \otimes_{n=1}^N \mathbf{U}_n \text{vec}(\mathcal{G})\|_F^2 + \beta \|\text{vec}(\mathcal{G})\|_1 \\ & := f(\mathcal{G}) + g(\mathcal{G}) \end{aligned} \quad (12)$$

which can be solved by the proximal gradient method.

Proposition 2: The objective function of subproblem (12) is the sum of two convex functions, and the gradient $\nabla_{\mathcal{G}} f(\mathcal{G})$ is Lipschitz continuous with the Lipschitz constant $L_{\mathcal{G}} = \|\otimes_{n=1}^N \mathbf{U}_n^T \mathbf{U}_n\|_2 = \prod_{n=1}^N \|\mathbf{U}_n^T \mathbf{U}_n\|_2$.

Based on *Proposition 2*, we denote the core tensor prox-linear function as (13)

$$\hat{\mathcal{G}} = \underset{\mathcal{G}}{\text{argmin}} \quad \left\langle \nabla_{\mathcal{G}} f(\tilde{\mathcal{G}}), \mathcal{G} - \tilde{\mathcal{G}} \right\rangle + \frac{L_{\mathcal{G}}}{2} \|\mathcal{G} - \tilde{\mathcal{G}}\|_F^2 + \beta \|\mathcal{G}\|_1, \quad (13)$$

where $\tilde{\mathcal{G}}$ denotes the extrapolated point. Using the soft-thresholding operator [35], the core tensor updating rule is shown as (14), and the detailed proof can be seen in Appendix A.

Thirdly, considering the core tensor \mathcal{G} is sparsity and interacts with all \mathbf{U}_n , our proposed algorithm applies the order of $\mathcal{G}, \mathbf{U}_1, \mathbf{U}_2, \dots, \mathbf{U}_N$ to speed up the convergence.

Suppose the current iteration is k -th step, we update the core tensor \mathcal{G}^k by

$$\mathcal{G}^{k+1} = \mathcal{S}_{\frac{\beta}{L_{\mathcal{G}}^k}} \left(\tilde{\mathcal{G}}^k - \frac{1}{L_{\mathcal{G}}^k} \nabla_{\mathcal{G}} f(\tilde{\mathcal{G}}^k) \right), \quad (14)$$

where $\tilde{\mathcal{G}}^k$ is updated by (37) and $\mathcal{S}_{\mu}(\mathcal{G})$ is a soft-thresholding operator defining component-wisely as

$$\mathcal{S}_{\mu}(x) = \text{sign}(x) \cdot \max(0, |x| - \mu).$$

Also, we update one latent factor matrices $\{\mathbf{U}_n^k\}$ using

$$\mathbf{U}_n^{k+1} = \mathcal{P}_+ \left(\tilde{\mathbf{U}}_n^k - \frac{1}{L_{\mathbf{U}_n^k}} \nabla_{\mathbf{U}_n} \ell(\tilde{\mathbf{U}}_n^k) \right), \quad (15)$$

where $\tilde{\mathbf{U}}_n^k$ is updated by (32) and $\mathcal{P}_+(\mathbf{U})$ is a mapping function that projects the negative entries of \mathbf{U} into zeros. We check whether the objective function (7) decreases during the APG projection. If so, we re-update \mathcal{G}^k and \mathbf{U}_n^k with the extrapolated point given by (21).

Technically, we propose an initial strategy where the $\{\mathbf{U}_n\}$ is generated randomly and then processed by normalization. Furthermore, at the end of iteration k , we apply the dynamic feedback correction mechanism to re-update tensor \mathcal{X}^k when having $\{\mathbf{U}_n^k\}$ and \mathcal{G}^k

$$\mathcal{X}^{k+1}_{\Omega} = \mathcal{X}^0_{\Omega} + \gamma(\mathcal{X}^k_{\Omega} - \mathcal{Z}^k_{\Omega}), \quad \mathcal{X}^{k+1}_{\bar{\Omega}} = \mathcal{Z}^k_{\bar{\Omega}}, \quad (16)$$

where $\mathcal{Z}^k = \mathcal{G}^k \times_1 \mathbf{U}_1^k \times_2 \cdots \times_N \mathbf{U}_N^k$, $\bar{\Omega}$ is the complement set of Ω , and $0 \leq \gamma \leq 1$ is a user defined hyper-parameter to control the correction. By doing these, we conclude that it can speed up the convergence and reduce the low-rank approximation errors.

Finally, if one of the following conditions is satisfied, we calculate the complete tensor $\hat{\mathcal{X}} = \mathcal{X}_{\Omega}^0 + \mathcal{Z}^{k+1}_{\bar{\Omega}}$ as the imputed result.

$$\begin{aligned} & \|\Omega \odot (\mathcal{Z}^k - \mathcal{X}^0)\|_F \|\Omega \odot \mathcal{X}^0\|_F^{-1} < \text{tol for some } k, \\ & \text{or} \\ & \frac{|\mathbb{F}_{\Omega}^k - \mathbb{F}_{\Omega}^{k+1}|}{1 + \mathbb{F}_{\Omega}^k} \leq \text{tol, for three consecutive } k \text{'s,} \end{aligned} \quad (17)$$

where \mathbb{F}_{Ω}^k denotes the objective function under observed index Ω at iteration k , and tol is a small specified positive value.

We conclude Algorithm 1 as the proposed APG-based updating procedure for ManiRTD problems. As seen in Algorithm 1, each variable is updated with a closed-form solution, which can improve the algorithm's efficiency.

B. Convergence Analysis

Since the ManiRTD problem is nonconvex, obtaining the optimal global solution is impossible. It is shown in [34] that (7) with cyclic block coordinate descent updating rule has global convergence to a stationary point. We provide the convergence property in **Theorem 1** for the ManiRTD algorithm.

Theorem 1. Let $\Theta^k = \{\{\mathbf{U}_n^k\}, \mathcal{G}^k\}$ be the sequence generated by Algorithm 1, and then we have the following conclusions.

- $\{\{\mathbf{U}_n^k\}, \mathcal{G}^k\}$ are all Cauchy sequences.

Algorithm 1 APG-based solver for the ManiRTD model

- 1: **Input:** Observed incomplete tensor $\mathcal{X}^0 \in \mathbb{R}_{+}^{I_1 \times I_2 \times \cdots \times I_N}$, Ω containing indices of observed entries, and the parameters α, β , tol, $0 \leq \gamma \leq 1$ and K .
- 2: **Output:** Complete tensor $\hat{\mathcal{X}}$ and latent factor matrices $\{\mathbf{U}_n^k\}_{n=1}^N$.
- 3: **construct** positive semi-definite similarity matrix \mathbf{W} and Toeplitz matrix \mathbf{T} ;
- 4: **initialize** $\mathcal{G}^0, \mathbf{U}_n^0 \in \mathbb{R}_{+}^{I_n \times I_n}$ ($1 \leq n \leq N$) and define \mathcal{Z}^0 as null tensor;
- 5: $\mathcal{X}_{\Omega} = \mathcal{X}^0_{\Omega}, \mathcal{X}_{\bar{\Omega}} = \mathcal{Z}^0_{\bar{\Omega}}$;
- 6: **for** $k = 1$ to K **do**
- 7: **for** $n = 1$ to N **do**
- 8: Optimize \mathcal{G} according to (14);
- 9: Optimize \mathbf{U}_n using (15);
- 10: **if** $\mathbb{F}(\mathcal{G}^n, \mathbf{U}_{j \leq n}, \mathbf{U}_{j > n})$ is decreasing **then**
- 11: Re-update $\mathcal{G}^{k,n}$ and \mathbf{U}_n^k respectively under extrapolated point given by (21);
- 12: **else**
- 13: Re-update $\mathcal{G}^{k,n}$ and \mathbf{U}_n^k respectively with $\tilde{\mathcal{G}}^k = \mathcal{G}^{k,n-1}$ and $\tilde{\mathbf{U}}_n^k = \mathbf{U}_n^{k-1}$;
- 14: **end if**
- 15: **end for**
- 16: Set $\mathcal{G}^k = \mathcal{G}^{k,N}$;
- 17: Update $\mathcal{Z}^k = \mathcal{G}^k \times_1 \mathbf{U}_1^k \times_2 \cdots \times_N \mathbf{U}_N^k$;
- 18: Implement dynamic feedback correction mechanism (16) for input tensor \mathcal{X}^k ;
- 19: **until** stopping conditions (17) are satisfied.
- 20: **end for**
- 21: **return** $\hat{\mathcal{X}}_{\Omega} = \mathcal{X}^0_{\Omega}, \hat{\mathcal{X}}_{\bar{\Omega}} = \mathcal{Z}^{k+1}_{\bar{\Omega}}$ and $\{\mathbf{U}_n^k\}_{n=1}^N$

- If hyper-parameters α, β are positive, then Θ^k converges to a stationary point $\hat{\Theta} = \{\{\tilde{\mathbf{U}}_n\}, \tilde{\mathcal{G}}\}$ of (7).

The above theorem ensures the feasibility of each solution produced by Algorithm 1. The proof of **Theorem 1** is based on the results of *Proposition 1* and *Proposition 2*. Firstly, the Cauchy sequence can be proven by showing the cost function of (7) is sufficient descent at each step, i.e., that $\sum_{k=2}^{\infty} \|\Theta^k - \Theta^{k+1}\|_F < \infty$. Then, we can prove $\hat{\Theta}$ is a stationary point by verifying the first-order optimality conditions. We omit the detail here, and please refer [35] to see the proof.

C. Computational Complexity Analysis

We analyze the computational complexity of the APG-based ManiRTD algorithm in this section. Since the Tucker decomposition algorithms compute the huge matrix multiplication and suffer from very high computational complexity, we combine the low-rank approximation with population Tucker decomposition strategies to reduce the computational complexity [36]. Throughout this section, we denote the input tensor as $\mathcal{X} \in \mathbb{R}^{I_1 \times \cdots \times I_N}$ and the core tensor as $\mathcal{G} \in \mathbb{R}^{r_1 \times \cdots \times r_N}$. Here are the results of the computational cost of core “shrinkage”, latent factor matrix updating rules, and completion procedure. The detailed analysis is shown in Appendix B.

Considering the proposed APG-based solver, gradient computing is the most time-consuming. Moreover, Lipschitz con-

stants calculation is negligible since the components can be obtained during the gradients' computation. So, guided by [35], the time complexity of core tensor updating is bounded by

$$\mathcal{O}\left(\sum_{n=1}^N\left(\prod_{i=1}^n r_i\right)\left(\prod_{j=n}^N I_j\right)\right),$$

and factor matrix updating requires

$$\mathcal{O}\left(\sum_{n=1}^N\left(\prod_{i=1}^n I_i\right)\left(\prod_{j=n}^N r_j\right)\right).$$

With the above analysis, assuming that the ManiRTD converges in the K iterations, we can roughly summarize the per-iteration complexity time complexity of the ManiRTD algorithm as

$$\mathcal{O}\left(\sum_{n=1}^N\left(\prod_{i=1}^n r_i\right)\left(\prod_{j=n}^N I_j\right) + N \sum_{n=1}^N\left(\prod_{i=1}^n I_i\right)\left(\prod_{j=n}^N r_j\right)\right), \quad (18)$$

where the per-iteration cost is relevant to the tensor sizes $\prod_{i=1}^n I_i$, the proposed algorithm is efficient theoretically.

VI. EXPERIMENTS

In this section, we conduct experiments on two different STDs to compare ManiRTD with baselines in different missing scenarios.

A. Traffic Datasets

We use the following two STDs for our experiment [37] and form them as 3rd/4th order tensors for traffic data imputation problems. Note that our Matlab codes are available on request.

- **(G):** Guangzhou urban traffic speed dataset. The original data is of size 214×8784 in the form of a multivariate time series matrix. We select seven days for our model training and reshape it into 4th order tensor $10 \times 205 \times 7 \times 1002$ and 3rd order tensor of size $214 \times 144 \times 7$.
- **(A):** Internet traffic flow dataset in Abilene. Dataset **A** includes 11 OD pairs, recording traffic flow every 5 minutes from December 8, 2003, to December 14, 2003. We can present dataset **A** as a 4th-order tensor $11 \times 11 \times 144 \times 7$. Also, we consider a third-order tensor of size $121 \times 144 \times 7$, where the first dimension corresponds to 121 OD pairs, the second to the time interval, and the last to 7 days.

B. Experimental Settings

1) *Missing scenario:* For a thorough verification of the ManiRTD to STDI problem, we take into account three missing scenarios, i.e., random missing (RM), structurally missing (SM), and black-out missing (BM). Generally, RM means that missing data is uniformly distributed, and SM is conducted by randomly selecting sensors and discarding consecutive hours. At the same time, BM refers to all sensors not working for a certain period of time. According to the mechanisms, we mask the observed index set Ω and use the partial observations for the model training.

2) *Baseline models:* For comparison, we select three state-of-the-art spatiotemporal traffic data imputation methods: LATC [4], LR-SETD [25], TAS-LR [13] and SRMF [8], to demonstrate the robustness and efficiency of our proposal. The baselines are shown in Tab. II, in which the TAS-LR and SRMF are matrix-based approaches, LATC is the matricization method, and LR-SETD is the tensor decomposition method.

TABLE II
COMPARISON OF BASELINE MODELS

Baselines	Spatiotemporal constraints			Structures
	Low rankness	Spatial	Temporal	
ManiRTD	✓	✓	✓	3rd/4th tensor
LATC [4]	✓		✓	3rd tensor
LR-SETD [25]	✓		✓	3rd tensor
TAS-LR [13]	✓	✓	✓	Matrix
SRMF [8]	✓	✓	✓	Matrix

✓ denotes the mentioned method has considered the constraint.

3) *Model performance:* To measure the imputation performance, we adopt three criteria, including root mean square error (RMSE), mean absolute percentage error (MAPE), and normalized mean absolute error (NMAE):

$$\begin{aligned} \text{MAPE} &= \frac{1}{n} \sum_{i=1}^n \left| \frac{y_i - \hat{y}_i}{y_i} \right| \times 100, \\ \text{RMSE} &= \sqrt{\frac{1}{n} \sum_{i=1}^n (y_i - \hat{y}_i)^2}, \\ \text{NMAE} &= \frac{\sum_{i=1}^n |y_i - \hat{y}_i|}{\sum_{i=1}^n |y_i|} \end{aligned} \quad (19)$$

where y_i and \hat{y}_i are actual values and imputed values, respectively.

C. Implementation Details

Ablation studies: To illustrate the multidimensionality of STDs, we first discuss the traffic tensor structure in our ManiRTD model using **G** dataset with the RM scenarios. In particular, we remove the spatiotemporal constraints in (7) and denote the 3-rd and 4-th order tensor models as **M1** and **M2**, respectively. Fig. 2 shows the model performance, it can be seen that the 3rd-order tensor structure covers richer spatial and temporal information. To further verify the validity of the spatiotemporal regularizations, we discuss the effect of the spatial and temporal constraints of ManiRTD. The results are shown in Fig. 3. On the one hand, the NMAE value in Fig. 3 (a) decreases and then stabilization for datasets **G** and **A** with the spatial neighbor p increasing. Also, the cumulative density distribution (CDF) along with increment rates (IRs) [13] in Fig. 3 (b) shows that traffic speed data has more temporal variations than traffic flow data. These results imply that the proposed spatiotemporal constraint matrix is essential for our STDI problems. On the other hand, Fig. 3 (c)- (d) compares the influence of spatiotemporal constraints for datasets **G** and **A**, respectively. We can observe that the spatiotemporal regularizations enhance the traffic data imputation performance, especially in the temporal direction.

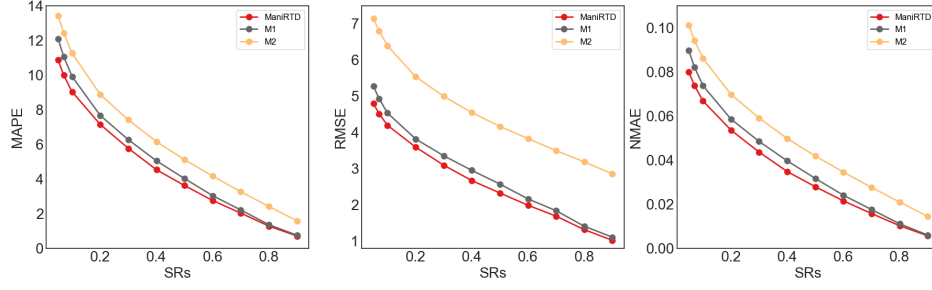


Fig. 2. Interpretation of the multidimensionality of STDs. The 3rd-order tensor structure performs better than the 4-th order tensor structure for dataset **G**.

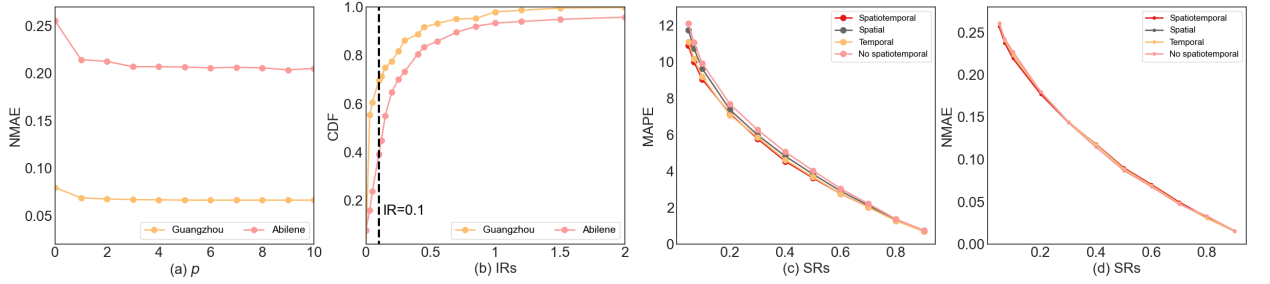


Fig. 3. Illustration of spatiotemporal constraints selection. (a) NMAE score by varying the neighbor number p for RM with 90% missing. (b) The cdf of traffic datasets rois. (c)-(d) Evaluation of the influence of spatiotemporal constraints for **G** and **A**, respectively.

Parameters setting: Two parameters α and β need to be tuned in our ManiRTD model. Hyperparameter α characterizes spatiotemporal regularization, β adjusts the strength of the sparsity term, i.e., the low-rank tensor approximation. In all our experiments, we set $\beta = 1$ and calculate the SVD ratios between mode- n unfolding matrices and spatiotemporal matrices to deliver α , such as $\alpha = 1e3 \times (0.26, 2.33, 2.45)$ for **G** under $SR = 0.05\%$. For better model comparison, the termination condition for all experiments is set to (17), where $tol = 10^{-5}$ and the maximum number of iterations is 300. Furthermore, the parameters of baselines are optimally assigned or automatically chosen as described in the reference papers.

Convergence behaviors: We have theoretically proven that the sequences generated by **Algorithm 1** converge to a stationary point in **Theorem 1**. Here, we show the numerical convergence of the proposed algorithm. Fig. 4 shows the curves of the relative error (RE) values versus the iteration number of the proposed ManiRTD on dataset **G**. Remark that the RE keeps decreasing as the iteration number increases, and the values stabilize after only about 250 iterations, which implies the proposed algorithm's numerical stability and convergence. Furthermore, we test the performance of RM under $SR = 0.05\%$, we can see that the proposed initialization strategy reduces the low-rank approximation errors, and the first-order control rule can speed up the convergence of the proposed algorithm.

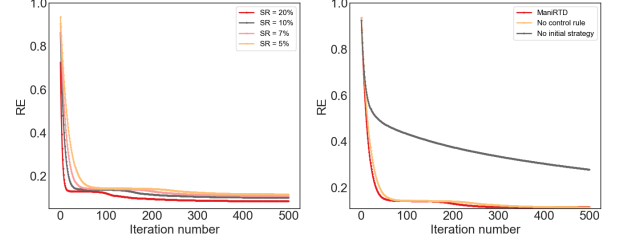


Fig. 4. The RE values versus the iteration number of the proposed ManiRTD on dataset **G**.

D. Results

This section will compare the ManiRTD method with other baselines mentioned in Tab. III.

1) *Overall performance among baseline models:* As mentioned above, the ablation studies show that spatial and temporal constraints can improve the imputation performance for the STDI problem. To show the superiority of the ManiRTD, Tab. III shows the overall imputation performance of baseline models on the datasets **G** and **A** under various missing scenarios. Of these results, NM and BM scenarios seem more challenging to reconstruct than the RM scenarios. Compared with other baselines, we can see that the ManiRTD model performs better in most cases.

To further compare the model performance of our proposal ManiRTD, we calculate the MAPE values for the **G** and NMAE values for the **A** under different RM scenarios (sample

TABLE III
PERFORMANCE COMPARISON OF MANIRTD AND OTHER BASELINES FOR RM, NM, AND BM SCENARIOS

Data	Missing scenario	ManiRTD	LATC	LR-SETD	TAS-LR	SRMF
G (RMSE/MAPE)	RM-30%	1.69/2.03	2.75/5.94	2.52/5.32	2.53/10.08	4.03/10.66
	RM-70%	3.09/5.71	3.17/6.93	3.25/6.89	3.33/11.62	4.83/12.39
	RM-90%	4.19/9.03	4.01/8.95	4.81/10.44	4.58/15.15	5.16/16.53
	RM-95%	4.79/10.88	6.25/12.59	7.98/16.21	5.61/17.69	6.81/19.06
	SM-30%	4.52/9.95	30.69/74.98	10.95/25.54	5.45/12.31	6.82/14.31
	SM-70%	10.24/16.22	36.59/88.01	12.45/27.45	12.80/19.14	15.72/24.71
	SM-90%	25.06/49.03	37.01/87.66	15.45/31.88	29.31/52.01	35.52/73.91
	BM-30%	13.46/27.76	20.91/45.66	10.63/28.02	18.41/32.65	24.57/52.18
A (NMAE)	RM-30%	0.0501	0.1229	0.1158	0.3092	0.3233
	RM-70%	0.1442	0.1488	0.1412	0.3178	0.3439
	RM-90%	0.2194	0.2228	0.2034	0.3407	0.3814
	RM-95%	0.2572	0.4809	0.2658	0.3576	0.3931
	SM-30%	0.2741	0.8969	0.6093	0.3214	0.4831
	SM-70%	0.4334	0.9611	0.7401	0.5791	0.6217
	SM-90%	0.7539	0.9902	0.8013	0.8176	0.8534
	BM-30%	0.5718	0.7089	0.9066	0.8417	0.9141

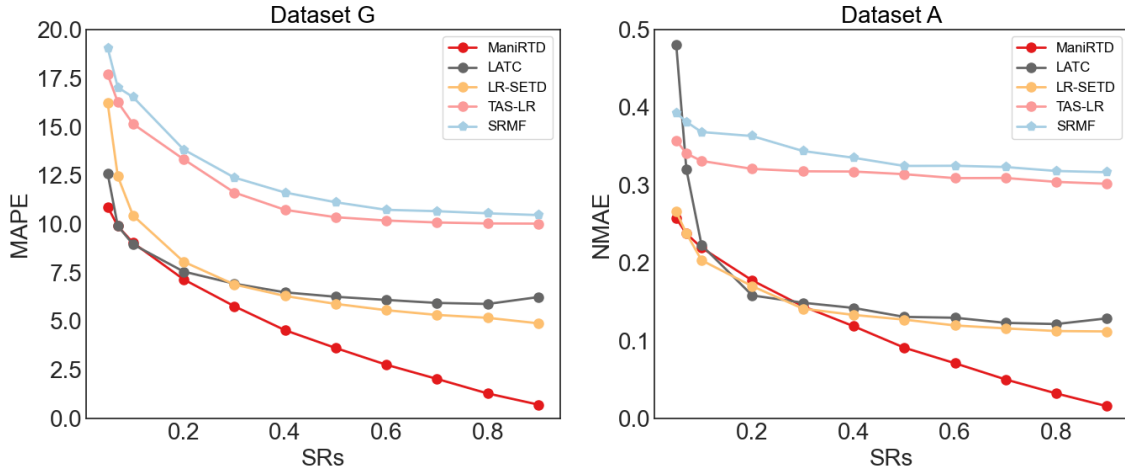


Fig. 5. MAPE and NMAE values for different sample ratios under RM scenarios for datasets **G** and **A** respectively.

ratio changed from 0.90 to 0.05) in Fig. 5. It is easy to see that ManiRTD has the lowest value, even for the extremely missing. Especially, the imputation with the MAPE value improvements is often higher than 5% when the missing rate is 95%. Compared with the dataset **G**, Fig. 6 shows that the errors for the dataset **A** are relatively higher; it can be inferred that traffic flow data have extreme points, such as close to 0 or rather huge, and then the imputing performance would accumulate relatively large errors. So, we conclude that the flow data variations are more unstable than speed data.

2) Imputation examples with different missing scenarios:

Here, we show some ManiRTD imputation examples with different missing scenarios on the Guangzhou (**G**) dataset. For the RM scenario, Fig. 7 shows the same signal trends under different sample ratios (see the number of purple dots), indicating that the ManiRTD can accurately impute partial observations. Also, the residuals in Fig. 8 reveal that the ManiRTD can successfully reconstruct the STD precisely, even for the extreme case (i.e., 90% RM). To further validate the superiority of our ManiRTD, we plot the structural missing scenarios (NM and BM) result in Fig. 9 and Fig. 10. In this

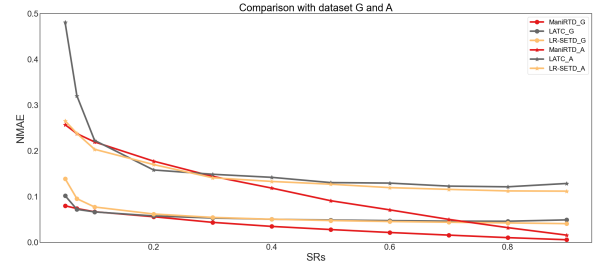


Fig. 6. NMAE value comparison with dataset **G** and **A** under RM scenarios.

case, the ManiRTD can achieve accurate imputation and learn traffic trends from severe missing scenarios.

VII. CONCLUSION

Spatiotemporal traffic data imputation (STDI) is an inevitable and challenging task in data-driven intelligent transportation systems (ITS). This paper treats the STDI as a low-

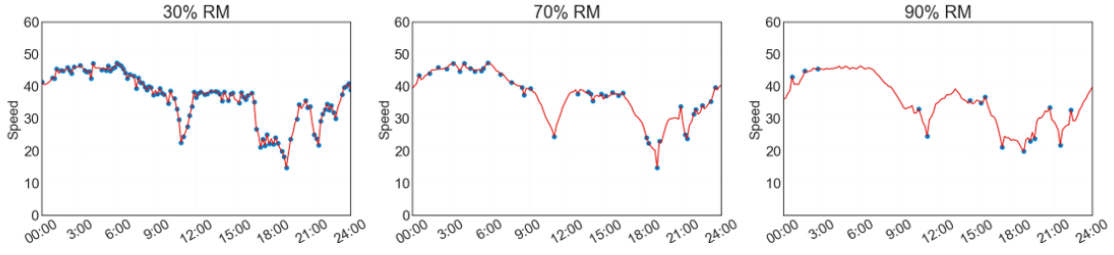


Fig. 7. Results of RM scenario on **G** dataset. This example corresponds to the 81st sensor and the 4th day of the dataset. Purple dots indicate the partially observed data, and red curves indicate the imputed values.

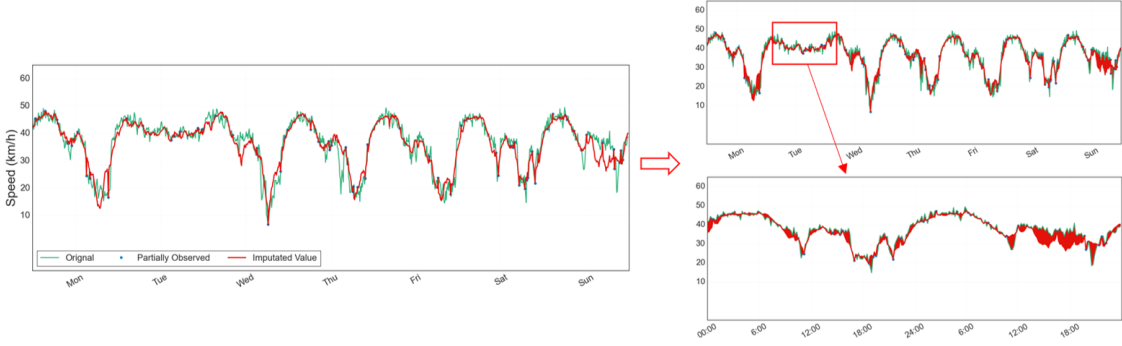


Fig. 8. Imputed values by ManiRTD on **G** dataset under RM scenario with 90% missing. Note that the red area (residual area) is only used to express the estimation performance, which does not represent the cumulative residual.

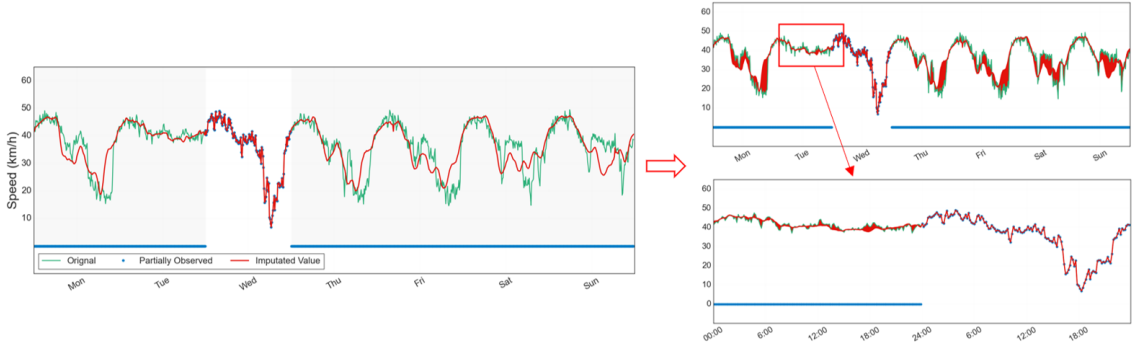


Fig. 9. Imputed values by ManiRTD on **G** dataset under NM scenario with 70% missing. The gray rectangles indicate the structural missing.

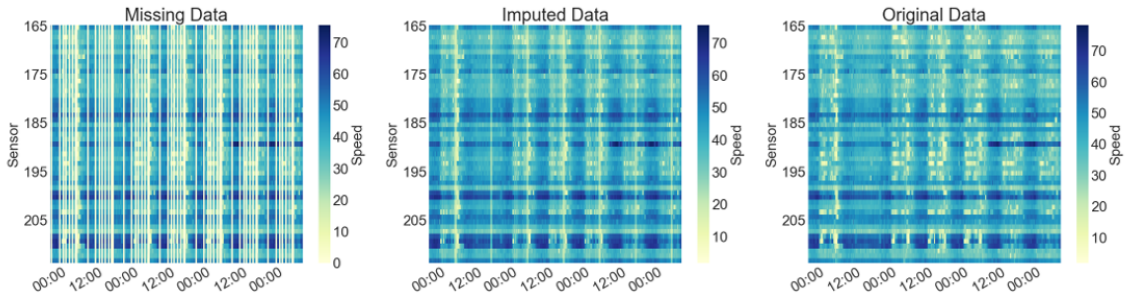


Fig. 10. The visualization of ManiRTD on **G** dataset under BM scenario with 30% missing. The middle heat map is our ManiRTD results.

rank Tucker approximation problem. The proposed ManiRTD exploits the global long-term trends using a low-rank Tucker model and captures the short-term patterns with manifold and Toeplitz regularizations. Through extensive experiments on spatiotemporal traffic datasets (STDs), our results show that

the proposed ManiRTD beats others for STDI with different RM scenarios, and leads to better performance on NM and BM missing scenarios (see Tab. III and Fig. 5).

There are three directions for future work. First, our proposal ignores the exact rank and uses a sparse regulariza-

tion term to promote low rankness. A potential approach is to use another low-rank tensor measure, such as applying the multiplication of the factor matrix rank to encode the Tucker rank [38]. Second, the current framework suffers a high computational cost for large-scale matrix multiplication calculations. One can consider the fast Fourier transform to address this issue [39]. Third, in addition to STDI, we can use the ManiRTD for spatiotemporal traffic data forecasting even with the missing observations [40]. Also, the proposed spatiotemporal traffic data modeling frameworks can be considered for urban traffic pattern discovery [41].

ACKNOWLEDGMENTS

The authors would like to thank the authors who shared their code and data on websites. This research is partly supported by Shenzhen Science and Technology Program (Grant No. ZDSYS20210623092007023, JCYJ20200109141218676).

APPENDIX A APG-BASED ALGORITHM FOR THE MANIRTD

Firstly, we denote the ManiRTD optimization problem as a class of regularized block multi-convex optimization problems:

$$\underset{\{\mathbf{x}_n\}}{\text{minimize}} \ell(\{\mathbf{x}_n\}) + \sum_{n=1}^N \alpha_n r_n(\mathbf{x}_n),$$

where $r_n(\mathbf{x}_n)$ is the given constraint. We consider the APG-based prox-linear operator to update every \mathbf{x}_n by solving a relaxed subproblem with a separable quadratic objective:

$$\mathbf{x}_n^k = \underset{\mathbf{x}_n}{\text{argmin}} \left\{ \langle \tilde{\mathbf{g}}^k, \mathbf{x}_n - \tilde{\mathbf{x}}_n^{k-1} \rangle + \frac{L_{\mathbf{x}_n}^{k-1}}{2} \|\mathbf{x}_n - \tilde{\mathbf{x}}_n^{k-1}\|_F^2 + \alpha_n r_n(\mathbf{x}_n) \right\}, \quad (20)$$

where $\tilde{\mathbf{x}}_n^{k-1}$ denotes an extrapolated point and update through

$$\begin{aligned} \tilde{\mathbf{x}}_n^{k-1} &= \mathbf{x}_n^{k-1} + \omega_{k-1} (\mathbf{x}_n^{k-1} - \mathbf{x}_n^{k-2}), \text{ for } k \geq 1 \\ \omega_{k-1} &= \frac{t^{k-2} - 1}{t^{k-1}}, \quad t^{k-1} = \frac{1 + \sqrt{4(t^{k-2})^2 + 1}}{2} \end{aligned} \quad (21)$$

and $\tilde{\mathbf{g}}^k = \nabla_{\mathbf{x}_n} \ell(\tilde{\mathbf{x}}_n^{k-1})$ is the partial gradient of objective function ℓ . Under the BCD framework with a given updating order, if $\tilde{\mathbf{g}}^k$ is Lipschitz continuous and exists the Lipschitz constant $L_{\mathbf{x}_n}$, then the updating rule (20) has global convergence to a stationary point [34].

Then we detail the proof of **Proposition 1** and **Proposition 2** as follows:

Proof of Proposition 1. Obviously, the Frobenius norm and matrix trace are differentiable functions. It remains to prove the convex property of ℓ and the Lipschitz continuous property of $\nabla_{\mathbf{U}_n} \ell$. Let $g = \frac{1}{2} \|\mathbf{X}_{(n)} - \mathbf{U}_n \mathbf{G}_{(n)} \mathbf{V}_n^T\|_F^2$ and $\mu = \text{tr}(\mathbf{U}_n^T \mathbf{L} \mathbf{U}_n)$ or $\|\mathbf{T} \mathbf{U}_n\|_F^2$, we have the gradient of $\ell(\mathbf{U}_n) = g(\mathbf{U}_n) + \frac{\alpha}{2} \mu(\mathbf{U}_n)$

$$\nabla_{\mathbf{U}_n} \ell(\mathbf{U}_n) = \mathbf{U}_n \mathbf{G}_{\mathbf{V}}^n \mathbf{G}_{\mathbf{V}}^{nT} - \mathbf{X}_{(n)} \mathbf{G}_{\mathbf{V}}^{nT} + \nabla_{\mathbf{U}_n} \mu(\mathbf{U}_n). \quad (22)$$

where $\mathbf{G}_{\mathbf{V}}^n = \mathbf{G}_{(n)} \mathbf{V}_n^T$ and $\mathbf{V}_n = (\otimes_{p \neq n}^1 \mathbf{U}_p)$.

In one hand, the Hessian matrix of $\ell(\mathbf{U}_n)$ is given by

$$\nabla_{\mathbf{U}_n}^2 \ell(\mathbf{U}_n) = \begin{cases} \mathbf{G}_{\mathbf{V}}^n \mathbf{G}_{\mathbf{V}}^{nT} + \alpha \mathbf{L}, & \text{Manifold} \\ \mathbf{G}_{\mathbf{V}}^n \mathbf{G}_{\mathbf{V}}^{nT} + \alpha \mathbf{T}^T \mathbf{T}, & \text{Temporal} \\ \mathbf{G}_{\mathbf{V}}^n \mathbf{G}_{\mathbf{V}}^{nT}, & \text{otherwise} \end{cases} \quad (23)$$

As we known, the functions $\mathbf{G}_{\mathbf{V}}^n \mathbf{G}_{\mathbf{V}}^{nT}$, \mathbf{L} and $\mathbf{T} \mathbf{T}^T$ are both positive semidefinite. According to the definition of a convex function, we know $\ell(\mathbf{U}_n)$ is convex.

On the other hand, we need the Lipschitz constant of $\nabla_{\mathbf{U}_n} \ell$. Since $\ell(\mathbf{U}_n)$ is a linear combination of $g(\mathbf{U}_n)$ and $\mu(\mathbf{U}_n)$, the Lipschitz constant of $\nabla_{\mathbf{U}_n} \ell$ can be calculated as a linear combination of the Lipschitz constants of the $\nabla_{\mathbf{U}_n} g$ and $\nabla_{\mathbf{U}_n} \mu$. Such as, the gradient of $\ell(\mathbf{U}_n) = g(\mathbf{U}_n) + \frac{\alpha}{2} \text{tr}(\mathbf{U}_n^T \mathbf{L} \mathbf{U}_n)$

$$\nabla_{\mathbf{U}_n} \ell(\mathbf{U}_n) = \mathbf{U}_n \mathbf{G}_{\mathbf{V}}^n \mathbf{G}_{\mathbf{V}}^{nT} - \mathbf{X}_{(n)} \mathbf{G}_{\mathbf{V}}^{nT} + \alpha \mathbf{L} \mathbf{U}_n. \quad (24)$$

For any two matrices $\mathbf{U}_n^1, \mathbf{U}_n^2$, we have

$$\begin{aligned} & \|\nabla_{\mathbf{U}_n} \ell(\mathbf{U}_n^1) - \nabla_{\mathbf{U}_n} \ell(\mathbf{U}_n^2)\|_F^2 \\ &= \left\| (\mathbf{U}_n^1 - \mathbf{U}_n^2) \mathbf{G}_{\mathbf{V}}^n \mathbf{G}_{\mathbf{V}}^{nT} - \alpha \mathbf{L} (\mathbf{U}_n^1 - \mathbf{U}_n^2) \right\|_F^2 \\ &\leq \left\| (\mathbf{U}_n^1 - \mathbf{U}_n^2) \mathbf{G}_{\mathbf{V}}^n \mathbf{G}_{\mathbf{V}}^{nT} \right\|_F^2 + \left\| \alpha \mathbf{L} (\mathbf{U}_n^1 - \mathbf{U}_n^2) \right\|_F^2. \end{aligned} \quad (25)$$

So, we only need to calculate the Lipschitz constant of the composite gradient $\nabla_{\mathbf{U}_n} \ell$ separately. More specifically,

$$\begin{aligned} & \left\| (\mathbf{U}_n^1 - \mathbf{U}_n^2) \mathbf{G}_{\mathbf{V}}^n \mathbf{G}_{\mathbf{V}}^{nT} \right\|_F^2 \\ &= \text{tr} \left(\mathbf{G}_{\mathbf{V}}^n \mathbf{G}_{\mathbf{V}}^{nT} (\mathbf{U}_n^1 - \mathbf{U}_n^2)^T (\mathbf{U}_n^1 - \mathbf{U}_n^2) \mathbf{G}_{\mathbf{V}}^n \mathbf{G}_{\mathbf{V}}^{nT} \right) \\ &\leq \left\| \mathbf{G}_{\mathbf{V}}^n \mathbf{G}_{\mathbf{V}}^{nT} \right\|_2^2 \|\mathbf{U}_n^1 - \mathbf{U}_n^2\|_F^2 \end{aligned} \quad (26)$$

and

$$\begin{aligned} & \left\| \alpha \mathbf{L} (\mathbf{U}_n^1 - \mathbf{U}_n^2) \right\|_F^2 \\ &= \text{tr} \left(\alpha \mathbf{L}^T (\mathbf{U}_n^1 - \mathbf{U}_n^2)^T (\mathbf{U}_n^1 - \mathbf{U}_n^2) \alpha \mathbf{L} \right) \\ &\leq \alpha \|\mathbf{L}\|_2^2 \|\mathbf{U}_n^1 - \mathbf{U}_n^2\|_F^2 \end{aligned} \quad (27)$$

where $\|\mathbf{G}_{\mathbf{V}}\|_2$ and $\|\mathbf{L}\|_2$ are the spectral norm with respect to $\mathbf{G}_{\mathbf{V}}$ and \mathbf{L} . Therefore, $\nabla_{\mathbf{U}_n} \ell(\mathbf{U}_n)$ is Lipschitz continuous and the Lipschitz constant is $L_{\mathbf{U}_n}$. Furthermore, the gradient of temporal regularization satisfies

$$\left\| \alpha \mathbf{T}^T \mathbf{T} (\mathbf{U}_n^1 - \mathbf{U}_n^2) \right\|_F^2 \leq \alpha \|\mathbf{T}^T \mathbf{T}\|_2^2 \|\mathbf{U}_n^1 - \mathbf{U}_n^2\|_F^2 \quad (28)$$

Combine with above Equations, we define the Lipschitz constant $L_{\mathbf{U}_n}$ as

$$L_{\mathbf{U}_n} = \begin{cases} \left\| \mathbf{G}_{\mathbf{V}}^n \mathbf{G}_{\mathbf{V}}^{nT} \right\|_2 + \alpha \|\mathbf{L}\|_2, & \text{Manifold} \\ \left\| \mathbf{G}_{\mathbf{V}}^n \mathbf{G}_{\mathbf{V}}^{nT} \right\|_2 + \alpha \|\mathbf{T}^T \mathbf{T}\|_2, & \text{Temporal} \\ \left\| \mathbf{G}_{\mathbf{V}}^n \mathbf{G}_{\mathbf{V}}^{nT} \right\|_2, & \text{otherwise} \end{cases} \quad (29)$$

This completes the proof.

To solve (11), we consider the Karush–Kuhn–Tucker (KKT) conditions as follows

$$\begin{aligned} \nabla_{\mathbf{U}_n} \Psi(\mathbf{U}_n, \tilde{\mathbf{U}}_n) &\geq 0, & \mathbf{U}_n &\geq 0 \\ \nabla_{\mathbf{U}_n} \Psi(\mathbf{U}_n, \tilde{\mathbf{U}}_n) \odot \mathbf{U}_n &= 0, \end{aligned} \quad (30)$$

where $\nabla_{\mathbf{U}_n} \Psi(\mathbf{U}_n, \tilde{\mathbf{U}}_n) = \nabla_{\mathbf{U}_n} \ell(\tilde{\mathbf{U}}_n) + L_{\mathbf{U}_n}(\mathbf{U}_n - \tilde{\mathbf{U}}_n)$ and \odot is the Hadamard product. By solving (30), we have

$$\mathbf{U}_n \leftarrow \mathcal{P}_+ \left(\tilde{\mathbf{U}}_n - \frac{1}{L_{\mathbf{U}_n}} \nabla_{\mathbf{U}_n} \ell(\tilde{\mathbf{U}}_n) \right), \quad (31)$$

where $\mathcal{P}_+(\mathbf{U})$ is the function that projects the negative entries of \mathbf{U} into zeros and $\tilde{\mathbf{U}}_n$ is updated by

$$\tilde{\mathbf{U}}_n^k = \mathbf{U}_n^k + \omega_k (\mathbf{U}_n^k - \mathbf{U}_n^{k-1}), \text{ for } k \geq 1 \quad (32)$$

with the update step size ω_k . \square

Proof of Proposition 2. As in Proposition 1, verifying the convex and Lipschitz continuous properties is straightforward. For the vectorization form, we have

$$\begin{aligned} \text{vec}(\nabla_{\mathcal{G}} f(\mathcal{G})) &= (\otimes_{n=N}^1 \mathbf{U}_n^T \mathbf{U}_n) \text{vec}(\mathcal{G}) \\ &\quad - (\otimes_{n=N}^1 \mathbf{U}_n^T) \text{vec}(\mathcal{X}), \end{aligned} \quad (33)$$

Then, the Hessian matrix $\text{vec}(\nabla_{\mathcal{G}}^2 f(\mathcal{G})) = \otimes_{n=N}^1 \mathbf{U}_n^T \mathbf{U}_n$, which is positive semidefinite and assures $f(\mathcal{G})$ is convex. Furthermore, we use the properties of Kronecker product to calculate $\nabla_{\mathcal{G}} f(\mathcal{G})$ as follows

$$\begin{aligned} \nabla_{\mathcal{G}} f(\mathcal{G}) &= \mathcal{G} \times_1 \mathbf{U}_1^T \mathbf{U}_1 \cdots \times_N \mathbf{U}_N^T \mathbf{U}_N \\ &\quad - \mathcal{X} \times_1 \mathbf{U}_1^T \cdots \times_N \mathbf{U}_N^T. \end{aligned} \quad (34)$$

For any given \mathcal{G}_1 and \mathcal{G}_2 , we have

$$\begin{aligned} &\|\text{vec}(\nabla_{\mathcal{G}} f(\mathcal{G}_1)) - \text{vec}(\nabla_{\mathcal{G}} f(\mathcal{G}_2))\|_F \\ &= \left\| \otimes_{n=N}^1 \mathbf{U}_n^T \mathbf{U}_n (\text{vec}(\mathcal{G}_1) - \text{vec}(\mathcal{G}_2)) \right\|_F \\ &\leq \left\| \otimes_{n=N}^1 \mathbf{U}_n^T \mathbf{U}_n \right\|_2 \|\text{vec}(\mathcal{G}_1) - \text{vec}(\mathcal{G}_2)\|_F \\ &= \prod_{n=1}^N \|\mathbf{U}_n^T \mathbf{U}_n\|_2 \|\text{vec}(\mathcal{G}_1) - \text{vec}(\mathcal{G}_2)\|_F. \end{aligned} \quad (35)$$

So, the Lipschitz constant of $\nabla_{\mathcal{G}} f(\mathcal{G})$ is $L_{\mathcal{G}} = \prod_{n=1}^N \|\mathbf{U}_n^T \mathbf{U}_n\|_2$. This completes the proof. \square

Based on the results given by Proposition 2, we can use the soft thresholding operator to solve the composite model (13), and the result is

$$\hat{\mathcal{G}} = T_{L_{\mathcal{G}}}^{f, \mathcal{G}}(\mathcal{G}) = \mathcal{S}_{\frac{\beta}{L_{\mathcal{G}}}} \left(\tilde{\mathcal{G}} - \frac{1}{L_{\mathcal{G}}} \nabla_{\mathcal{G}} f(\tilde{\mathcal{G}}) \right), \quad (36)$$

where $\mathcal{S}_{\zeta}(\cdot)$ is ‘shrinkage’ operator and $\tilde{\mathcal{G}}$ is updated by

$$\tilde{\mathcal{G}}^k = \mathcal{G}^k + \omega_k (\mathcal{G}^k - \mathcal{G}^{k-1}), \text{ for } k \geq 1 \quad (37)$$

with the update step size ω_k .

APPENDIX B

COMPUTATIONAL COMPLEXITY ANALYSIS

Here, we analyze the computational complexity of the proposed ManiRTD. Suppose that $\mathcal{X} \in \mathbb{R}^{I_1 \times \dots \times I_N}$ and the core tensor $\mathcal{G} \in \mathbb{R}^{r_1 \times \dots \times r_N}$, we have the basic computational complexity: the computational cost of $\mathbf{U}_n^T \mathbf{U}_n$ is $\mathcal{O}(r_n^2 I_n)$ and the mode-n product with the matrix \mathbf{U}_n of tensor \mathcal{G} is $\mathcal{O}(\sum_{n=1}^N \prod_{i=1}^n I_i \prod_{i=1}^N r_i)$. Furthermore, we reformulate the Kronecker product in $\mathbf{G}_{\mathbf{V}}^n = \mathbf{G}_{(n)} \mathbf{V}_n^T$ but let

$$\mathcal{Y} = \mathcal{G} \times_1 \mathbf{U}_1 \cdots \times_{n-1} \mathbf{U}_{n-1} \times_{n+1} \mathbf{U}_{n+1} \cdots \times_N \mathbf{U}_N,$$

such that we have $\mathbf{G}_{\mathbf{V}}^n = \mathcal{Y}_{(n)}$ and its computational cost is

$$\begin{aligned} \mathcal{O}(\mathbf{G}_{\mathbf{V}}^n) &= \mathcal{O} \left(\sum_{j=1}^{n-1} \left(\prod_{i=1}^j I_i \right) \left(\prod_{i=j}^N r_i \right) \right) + \\ &\quad \mathcal{O} \left(r_n \left(\prod_{i=1}^{n-1} I_i \right) \sum_{j=n+1}^N \left(\prod_{i=n+1}^j I_i \right) \left(\prod_{i=j}^N r_i \right) \right) \\ &\leq \mathcal{O} \left(\sum_{n=1}^N \left(\prod_{i=1}^n I_i \right) \left(\prod_{j=n}^N r_j \right) \right) \end{aligned} \quad (38)$$

Also, we conclude that the computational cost of tensor unfolding, soft-thresholding operator, and projection to non-negative is negligible compared to gradient computing.

Considering the proposed APG-based optimization for core tensor ‘shrinkage’, the computation of $\nabla_{\mathcal{G}} f(\mathcal{G})$ requires

$$\mathcal{O} \left(\sum_{n=1}^N r_n^2 I_n + \sum_{n=1}^N r_n \prod_{i=1}^N r_i + \sum_{n=1}^N \left(\prod_{i=1}^n r_i \right) \left(\prod_{j=n}^N I_j \right) \right). \quad (39)$$

where the first part comes from the computation of all $\mathbf{U}_n^T \mathbf{U}_n$, and the second and third parts are respectively, from the computations of the first and second terms in (34).

Similarly, we use (38) to calculate the computational complexity of $\nabla_{\mathbf{U}_n} \ell(\mathbf{U}_n)$ and requires

$$\mathcal{O} \left(r_n^2 \left(\prod_{i \neq n} I_i \right) + r_n^2 I_n \right) + \mathcal{O} \left(\prod_{i=1}^n I_i \right) + \mathcal{O}(r_n^3) + \mathcal{O}(\mathbf{G}_{\mathbf{V}}^n). \quad (40)$$

The first three parts are from the computations of the three terms in (22).

Since $r_n < I_n$ for all $n = 1, \dots, N$, the value of (39) and (40) are dominated by the last part, respectively. So, the computational cost of $\nabla_{\mathcal{G}} f(\mathcal{G})$ is

$$\mathcal{O} \left(\sum_{n=1}^N \left(\prod_{i=1}^n r_i \right) \left(\prod_{j=n}^N I_j \right) \right). \quad (41)$$

and $\nabla_{\mathbf{U}_n} \ell(\mathbf{U}_n)$ is

$$\mathcal{O} \left(\sum_{n=1}^N \left(\prod_{i=1}^n I_i \right) \left(\prod_{j=n}^N r_j \right) \right). \quad (42)$$

REFERENCES

- [1] X. Chen, Z. He, and J. Wang, ‘‘Spatial-temporal traffic speed patterns discovery and incomplete data recovery via SVD-combined tensor decomposition,’’ *Transportation Research Part C: Emerging Technologies*, vol. 86, pp. 59–77, 2018.
- [2] S. Moritz and T. Bartz-Beielstein, ‘‘imputeTS: Time Series Missing Value Imputation in R,’’ *The R Journal*, vol. 9, no. 1, pp. 207–218, 2017.
- [3] T. Thomas and E. Rajabi, ‘‘A systematic review of machine learning-based missing value imputation technique,’’ *Data Technologies and Applications*, 2021.
- [4] X. Chen, M. Lei, N. Saunier, and L. Sun, ‘‘Low-rank autoregressive tensor completion for spatiotemporal traffic data imputation,’’ *IEEE Transactions on Intelligent Transportation Systems*, pp. 1–10, 2021.
- [5] Q. Song, H. Ge, J. Caverlee, and X. Hu, ‘‘Tensor completion algorithms in big data analytics,’’ *ACM Trans. Knowl. Discov. Data*, vol. 13, no. 1, p. 48, 2019.

- [6] T. G. Kolda and B. W. Bader, "Tensor decompositions and application," *SIAM Review*, vol. 5, no. 3, p. 455–500, 2009.
- [7] M. T. Bahadori, Q. R. Yu, and Y. Liu, "Fast multivariate spatio-temporal analysis via low rank tensor learning," in *Neural Information Processing Systems (NIPS)*, 2014, p. 3491–3499.
- [8] M. Roughan, Y. Zhang, W. Willinger, and L. Qiu, "Spatio-temporal compressive sensing and internet traffic matrices (extended version)," *IEEE/ACM Transactions on Networking*, vol. 20, no. 3, pp. 662–676, 2012.
- [9] A. B. Said and A. Erradi, "Spatiotemporal tensor completion for improved urban traffic imputation," *IEEE Transactions on Intelligent Transportation Systems*, pp. 1–14, 2021.
- [10] X. Wang, Y. Wu, D. Zhuang, and L. Sun, "Low-rank Hankel tensor completion for traffic speed estimation," *IEEE Transactions on Intelligent Transportation Systems*, vol. 24, no. 5, pp. 4862–4871, 2023.
- [11] X. Li, M. K. Ng, G. Cong, Y. Ye, and Q. Wu, "MR-NTD: Manifold regularization nonnegative Tucker decomposition for tensor data dimension reduction and representation," *IEEE Transactions on Neural Networks and Learning Systems*, vol. 28, no. 8, pp. 1787–1800, 2017.
- [12] A. Narita, K. Hayashi, R. Tomioka, and H. Kashima, "Tensor factorization using auxiliary information," *Data Mining and Knowledge Discovery*, vol. 25, p. 298–324, 2012.
- [13] Y. Wang, Y. Zhang, X. Piao, H. Liu, and K. Zhang, "Traffic data reconstruction via adaptive spatial-temporal correlations," *IEEE Transactions on Intelligent Transportation Systems*, vol. 20, no. 4, pp. 1531–1543, 2019.
- [14] P. Wu, L. Xu, and Z. Huang, "Imputation methods used in missing traffic data: A literature review," in *Artificial Intelligence Algorithms and Applications*, 2020, pp. 662–677.
- [15] E. J. Candes and B. Recht, "Exact matrix completion via convex optimization," *Foundations of Computational Mathematics*, vol. 9, no. 6, p. 717–772, 2009.
- [16] J. Liu, P. Musialski, P. Wonka, and J. Ye, "Tensor completion for estimating missing values in visual data," *IEEE Transactions on Pattern Analysis and Machine Intelligence*, vol. 35, no. 1, pp. 208–220, 2013.
- [17] B. Ran, H. Tan, Y. Wu, and P. J. Jin, "Tensor based missing traffic data completion with spatial-temporal correlation," *Physica A : Statistical Mechanics and its Applications*, vol. 446, pp. 54–63, 2016.
- [18] T. Yokota, B. Erem, S. Guler, S. K. Warfield, and H. Hontani, "Missing slice recovery for tensors using a low-rank model in embedded space," in *IEEE/CVF Conference on Computer Vision and Pattern Recognition (CVPR)*, 2018, pp. 8251–8259.
- [19] Q. Shi, J. Yin, J. Cai, A. Cichocki, T. Yokota, L. Chen, M. Yuan, and J. Zeng, "Block Hankel tensor ARIMA for multiple short time series forecasting," in *AAAI Conference on Artificial Intelligence (AAAI)*, vol. 30, no. 04, 2020, pp. 5758–5766.
- [20] H. Tan, G. Feng, J. Feng, W. Wang, Y.-J. Zhang, and F. Li, "A tensor-based method for missing traffic data completion," *Transportation Research Part C: Emerging Technologies*, vol. 28, pp. 15–27, 2013.
- [21] H. Tan, J. Feng, Z. Chen, F. Yang, and W. Wang, "Low multilinear rank approximation of tensors and application in missing traffic data," *Advances in Mechanical Engineering*, vol. 6, pp. 1575–1597, 2014.
- [22] Y. Wang, Y. Zheng, and Y. Xue, "Travel time estimation of a path using sparse trajectory," in *20th ACM SIGKDD international conference on Knowledge discovery and data mining*, 2014, pp. 25–34.
- [23] X. Chen, Z. He, and L. Sun, "A Bayesian tensor decomposition approach for spatiotemporal traffic data imputation," *Transportation Research Part C: Emerging Technologies*, vol. 98, pp. 73–84, 2019.
- [24] Y. Wu, H. Tan, Y. Li, J. Zhang, and X. Chen, "A fused CP factorization method for incomplete tensors," *IEEE Transactions on Neural Networks and Learning Systems*, vol. 30, no. 3, pp. 751–764, 2019.
- [25] C. Pan, C. Ling, H. He, L. Qi, and Y. Xu, "Low-rank and sparse enhanced Tucker decomposition for tensor completion," *arXiv*, vol. abs/2010.00359, 2020.
- [26] H.-F. Yu, N. Rao, and I. S. Dhillon, "Temporal regularized matrix factorization for high-dimensional time series prediction," in *Neural Information Processing Systems (NIPS)*, 09 2016.
- [27] J. H. de Morais Goulart and G. Favier, "Low-rank tensor recovery using sequentially optimal modal projections in iterative hard thresholding," *SIAM Journal on Scientific Computing*, vol. 39, no. 3, pp. 860–889, 2017.
- [28] H. Zhang, P. Chen, J. Zheng, J. Zhu, G. Yu, Y. Wang, and H. X. Liu, "Missing data detection and imputation for urban ANPR system using an iterative tensor decomposition approach," *Transportation Research Part C: Emerging Technologies*, vol. 107, pp. 337–355, 2019.
- [29] J. Wang, J. Wu, Z. Wang, F. Gao, and Z. Xiong, "Understanding urban dynamics via context-aware tensor factorization with neighboring regularization," *IEEE Transactions on Knowledge and Data Engineering*, vol. 32, no. 11, pp. 2269–2283, 2020.
- [30] J. H. Goulart, A. Kibangu, and G. Favier, "Traffic data imputation via tensor completion based on soft thresholding of Tucker core," *Transportation Research Part C Emerging Technologies*, vol. 85, pp. 348–362, 12 2017.
- [31] X. Chen, "Bayesian temporal factorization for multidimensional time series prediction," Apr. 2021. [Online]. Available: <https://doi.org/10.5281/zenodo.4693405>
- [32] J. J.-Y. Wang, H. Bensmail, and X. Gao, "Multiple graph regularized nonnegative matrix factorization," *Pattern Recognition*, vol. 46, no. 10, pp. 2840–2847, 2013.
- [33] T. K. Sinha, J. Naram, and P. Kumar, "Nonnegative low-rank tensor completion via dual formulation with applications to image and video completion," in *Proceedings of the IEEE/CVF Winter Conference on Applications of Computer Vision (WACV)*, January 2022, pp. 3732–3740.
- [34] Y. Xu and W. Yin, "A Block Coordinate Descent method for regularized multiconvex optimization with applications to nonnegative tensor factorization and completion," *SIAM Journal on Imaging Sciences*, vol. 6, no. 3, pp. 1758–1789, 2013.
- [35] Y. Xu, "Alternating proximal gradient method for sparse nonnegative Tucker decomposition," *Mathematical Programming Computation*, vol. 5, no. 3, p. 455–500, 2015.
- [36] G. Zhou, A. Cichocki, Q. Zhao, and S. Xie, "Efficient nonnegative Tucker decompositions: Algorithms and uniqueness," *IEEE Transactions on Image Processing*, vol. 24, no. 12, pp. 4990–5003, 2015.
- [37] W. Gong, "ManiRTD," Mar. 2023. [Online]. Available: <https://doi.org/10.5281/zenodo.7725126>
- [38] Q. Xie, Q. Zhao, D. Meng, and Z. Xu, "Kronecker-basis-representation based tensor sparsity and its applications to tensor recovery," *IEEE Transactions on Pattern Analysis and Machine Intelligence*, vol. 40, no. 8, pp. 1888–1902, 2018.
- [39] R. Yamamoto, H. Hontani, A. Imakura, and T. Yokota, "Fast algorithm for low-rank tensor completion in delay-embedded space," in *2022 IEEE/CVF Conference on Computer Vision and Pattern Recognition (CVPR)*, 2022, pp. 2048–2056.
- [40] X. Chen and L. Sun, "Bayesian temporal factorization for multidimensional time series prediction," *IEEE Transactions on Pattern Analysis and Machine Intelligence*, vol. 44, no. 9, pp. 4659–4673, 2022.
- [41] X. Chen, C. Zhang, X. Chen, N. Saunier, and L. Sun, "Discovering dynamic patterns from spatiotemporal data with time-varying low-rank autoregression," *arXiv*, vol. abs/2211.15482, 2022.



Wenwu Gong is currently pursuing a Ph.D. degree in the Department of Statistics and Data Science at Southern University of Science and Technology, Shenzhen, China. He received his B.S. in Mathematics from the Harbin Institute of Technology, Harbin, China. His research interests include spatiotemporal data mining, tensor learning, and machine learning.



Zhejun Huang is a research assistant professor in the Department of Statistics and Data Science at the Southern University of Science and Technology (SUSTech). He obtained his Ph.D. in mathematics in 2017 from the University of New South Wales (UNSW), Australia. He was a postdoctoral fellow at UNSW and Shenzhen Institutes of Advanced Technology (SIAT), Chinese Academy of Sciences. His research interests include big data analysis, mathematical modeling, and numerical optimization.



Lili Yang is working in the Mathematics Department at Southern University of Science and Technology as a full-time professor. She has a master's and Ph.D. in computer science from the UK and is a certified IT specialist with the national computer society. Her research interests include big data analysis, machine learning, AI, and Multi-objective optimization.